High-energy spin waves in the linear-chain antiferromagnet $KFeS_2$

D. Welz,* M. Kohgi, and Y. Endoh
Department of Physics, Faculty of Science, Tohoku University, Aramaki, Aoba-ku, Sendai 980, Japan

M. Nishi
Institute for Solid State Physics, University of Tokyo, Roppongi, Minato-ku, Tokyo 106, Japan

M. Arai†
ISIS Facility, Rutherford Appleton Laboratory, Chilton, Didcot, Oxfordshire, England
(Received 30 December 1991)

The chopper spectrometer MARI at the ISIS pulsed neutron source was used to measure the spin-wave dispersion in the Heisenberg linear-chain antiferromagnet $KFeS_2$ at 10.7 K. Aligning the chain axis of a 3.4-cm^3 single crystal with the direction of incidence allowed the signal to be integrated over all low-angle detectors ($2\theta < \approx 10°$) without significant loss of resolution. To extract the spin-wave energies, peaks in the time-of-flight scans were fitted with Gaussian profiles, and the corresponding longitudinal momentum transfers were obtained as averages over the active detector area with weighting for the signal dependence on the spin orientation and form factor. The resulting data points are well described by $E(k)=[A^2+B^2\sin^2(Ck)]^{1/2}$, with $A=41(7)$ meV, $B=217(4)$ meV, and $C=2.686(4)$ Å, implying a zone-boundary energy of 221(4) meV, which is about twice the value extrapolated from earlier measurements with reactor thermal neutrons. The magnon gap of 41(7) meV can be attributed to the interchain dispersion averaged over the detector area. From a sudden disappearance of the zone-boundary signal for increasing incident energy, the magnon linewidth in the Néel state is seen to be less than about ±10 meV.

I. INTRODUCTION

An early measurement[1] of spin-wave energies in the Heisenberg linear-chain antiferromagnet $KFeS_2$ with thermal neutrons from a reactor has been put into doubt by a similar, recent determination[2] for $TlFeS_2$, yielding a roughly two times higher spin-wave velocity in the Fe-S tetrahedral chains that are a common feature of both compounds (Fig. 1). The zone-boundary energy extrapolated from the $TlFeS_2$ data[2] is close to 200 meV, and utterly beyond the reach of thermal neutron sources. Since successful experiments with elemental cobalt[3] made direct-geometry chopper spectrometers situated at the ISIS pulsed spallation source appear well adapted to measurements in this energy range, we have investigated[4] the upper part of the $KFeS_2$ spin-wave dispersion on the recently installed MARI spectrometer.[5]

There is a special advantage to measuring one-dimensional (1D) systems on this type of spectrometer, akin to the greater freedom available for focusing with a 1D sample on a triple-axis instrument: If the excitations exhibit a dispersion that is (locally) flat in directions perpendicular to the incident beam, the signal can be integrated over (part of) the low-angle detector area. A quasi-1D crystal aligned with the direction of incidence shows a dispersion depending solely on the longitudinal momentum transfer, and is therefore a most favorable choice, comparable to the case of nondispersive crystal-field excitations. Thus, at ISIS, epithermal spin-wave measurements should be feasible with samples of conventional ($\approx cm^3$) size.

Apart from the chain thioferrates being excellent candidates for testing this at energies where chopper spectrometers at a spallation source show their strength, a determination of the upper part of the spin-wave dispersion is of interest in its own right. From most of the other quasi-1D magnets studied,[6,7] the compounds are distinguished by a pronounced covalency in the Fe-S

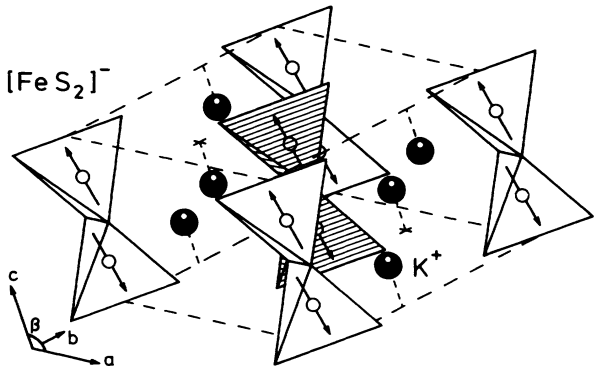

FIG. 1. $C2/c$ crystallographic structure of $KFeS_2$ with Fe-S tetrahedral chains lying in the monoclinic a-c plane. Antiferromagnetic order sets in below 250 K, leading to low-temperature moments of $2.43(3)\mu_B$ tilted 13(1)° from the chain axis within the monoclinic plane (Ref. 8).

tetrahedral chains (Fig. 1) which should account for the very strong exchange interactions as well as for the magnetic moments falling substantially short of the Fe^{3+} ionic value.[8-10] The effects appear to arise[2] largely from direct Fe-Fe contact between edge-sharing tetrahedra, thereby opening the possibility of differences in the exchange constants for compounds with different intrachain Fe separation (similar to differences observed among the ordered moments[8-10]), and of deviations from a local-moment behavior consequent on the electronic itinerancy (an activation behavior of the $KFeS_2$ electrical conductivity[11] indicates that the chains develop an antiferromagnetic band gap).

Thus, our investigation of $KFeS_2$ on MARI endeavored to check whether a well-defined spin-wave dispersion extends to the zone boundary, and then aimed for an accurate determination of the zone-boundary energy and for information on the magnon linewidth. The present account documents the results with emphasis on those aspects of experiment and analysis that are characteristic of the unfamiliar technique.

II. EXPERIMENT

Bulk crystalline $KFeS_2$ is opaque and of dark, gray-violet color, the dim shine of cleavage planes hardly giving a metallic impression. Literature crystallographic and magnetic data are collected in Table I. Because of the sizable zero-point fluctuation in quasi-1D antiferromagnets,[14,15] the intrinsic spin will be higher than indicated by the ordered magnetic moment, the calculated reduction[2] $\Delta S \approx 0.56$ for $TlFeS_2$ suggesting a value between $S=\frac{3}{2}$ and 2 in $KFeS_2$. Our single-crystal sample was 3.4 cm^3 in size (8.8 g), moderately elongated in the chain, or c, direction, and on a triple-axis spectrometer (TUNS at JRR-2, JAERI) showed a mosaic spread of approximately 2° in the chain axis. The sample was affixed to a small platform at the end of an aluminum rod, by means of a ∩-shaped strip cut from a thin aluminum sheet. Those parts of the assembly that did not need to be exposed to the neutron beam, including screws and a Rh-Fe resistor for thermometry, were surrounded by a cylindrical sheet of cadmium metal.

The sample assembly was attached to a closed-cycle refrigerator and loaded into a three-circle goniometer with ±6° variation, which, in turn, was installed on MARI.[5] This instrument (during test operation) was equipped with three out of eight low-angle detector banks (up, down, and left, as viewed from the sample). After removal of the Fermi chopper, the chain axis was aligned with the direction of incidence by equalizing the intensities of the lowest ($hk0$) Bragg reflections observed in a white beam. Time-of-flight (TOF) spectra were then accumulated at a sample temperature $T=10.7$ K for nominal incident-neutron energies E_i of 100, 200, 300, 400, and 450 meV over ≈1000 μA h protons, and for $E_i=500$ meV over ≈1500 μA h protons, a Ta backup target being employed for neutron production (mean incident proton current ≈100 μA). Standard rotors designated for 200 (B) and 500 meV (A) were used in the Fermi chopper and spun with 400 (B), 600 (B), 500 (A), 550 (A), 550 (A), and 600 Hz (A), respectively; the actual incident energies, as determined from monitor counter signals, are found in Table II. Finally, the run with nominal $E_i=300$ meV was repeated at room temperature (≈700 μA h protons).

The low-temperature spectra of $KFeS_2$ are shown in Fig. 2, where the signals from all detectors with scattering angle below ≈10° have been combined. In order to understand the spectra, it is sufficient, however, to consider the TOF signal picked up by an imaginary point detector in the forward direction. As a function of momentum transfer k, the neutron energy loss to the sample is given by $E=E_i-(\hbar^2/2m)(k_i-k)^2$, and peaks appear in the detected spectra at energies where this parabola (TOF scan) intersects the 1D dispersion curve (see Fig. 4). An important factor here is the characteristic weak-strong alternation in the antiferromagnetic spin-wave scattering cross section,[16] leading to a hardly detectable signal for wave vectors close to even multiples of $2\pi/c$, while near the odd-numbered dispersion minima a $1/E$ decrease in the cross section with increasing spin-wave energy E is predicted. The smooth tails extending upward from the elastic peak should be attributed to multiple phonon scattering.

Because of the usual periodic property of the 1D dispersion, similar information may be obtained for different incident energies E_i, with the choice bearing on signal resolution and intensity. Thus, the primary intensity from the moderator (liquid methane at 100 K) decaying approximately like $1/E_i$ in conjunction with the energy resolution (FWHM) of the spectrometer (with stan-

TABLE I. Crystallographic and magnetic data of $KFeS_2$ from x-ray and neutron diffraction, respectively. The Fe-S tetrahedral chains lie parallel with the c axis. Covalency in the chains makes a major contribution to the low value of the ordered magnetic moment.

	Lattice constants (295 K)				
Lattice symmetry	a (Å)	b (Å)	c (Å)	β (deg)	Ref.
Monoclinic $C2/c$	7.09	11.27	5.39	113.2	12,13

Néel temperature (K)	Ordered magnetic moment (μ_B)	Ordering direction (deg)	Ref.
250(1)	2.43(3)	13(1) from chain	8,9

dard rotors) increasing[5] from roughly 2% of E_i at $E=0$ to 1% at $E=E_i$, as well as a smaller background from multiple phonon scattering, suggest to take E_i as low as possible and use a correspondingly large k. For magnetic systems, however, a limit is often set by a rapid drop in form factor, demanding a compromise in dependence on sample size and magnetic scattering cross section. In accordance with the above, in the first dispersion minimum of $KFeS_2$ the spin-wave signal is strong but unresolved, in the third it is fully resolved into double peaks, and beyond this it becomes too weak (Fig. 2).

When, in practice, the signal is integrated over an extended detector area, the longitudinal and transverse momentum-transfer components as functions of the scattering angle 2θ are

$$k_{\parallel}=k_i-k_f\cos 2\theta, \quad k_{\perp}=k_f\sin 2\theta \ . \tag{1}$$

Because the final energies $E_f=(\hbar^2/2m)k_f^2$ are often large, $k_{\parallel}$ varies noticeably across the detector, so that (unlike the nondispersive case) there is an integration penalty even for a strictly 1D dispersion, and the variation in the magnetic form factor with $k_{\perp}$ becomes noticeable below $2\theta\approx 10°$ as well, thus (as in the nondispersive case) affecting the integration. Although for the present measurements the integration out to $2\theta\approx 10°$ causes no serious loss in resolution, the variation in $k_{\parallel}$ demands consideration if the intrinsic precision of the instrument is to be utilized fully. We have here used the following stepwise deconvolution to derive the spin-wave dispersion from the TOF spectra.

III. SIGNAL DECONVOLUTION

As a first step, presumed spin-wave peaks in the TOF spectra were least-squares fitted[17] with Gaussian profiles, where each peak was extracted separately above a linear sloping background, from finely binned data. The description by simple Gaussians turns out to be satisfactory even for the unresolved strong peaks from the first dispersion minimum, and the widths of the resolved and unambiguous peaks, ranging from $2\sigma\approx 1$ to ≈ 10 meV in dependence of E_i and E, are in reasonable agreement with the predicted spectrometer resolution.[5] Table II lists all the peaks that allowed stable fits with an acceptable peak width.

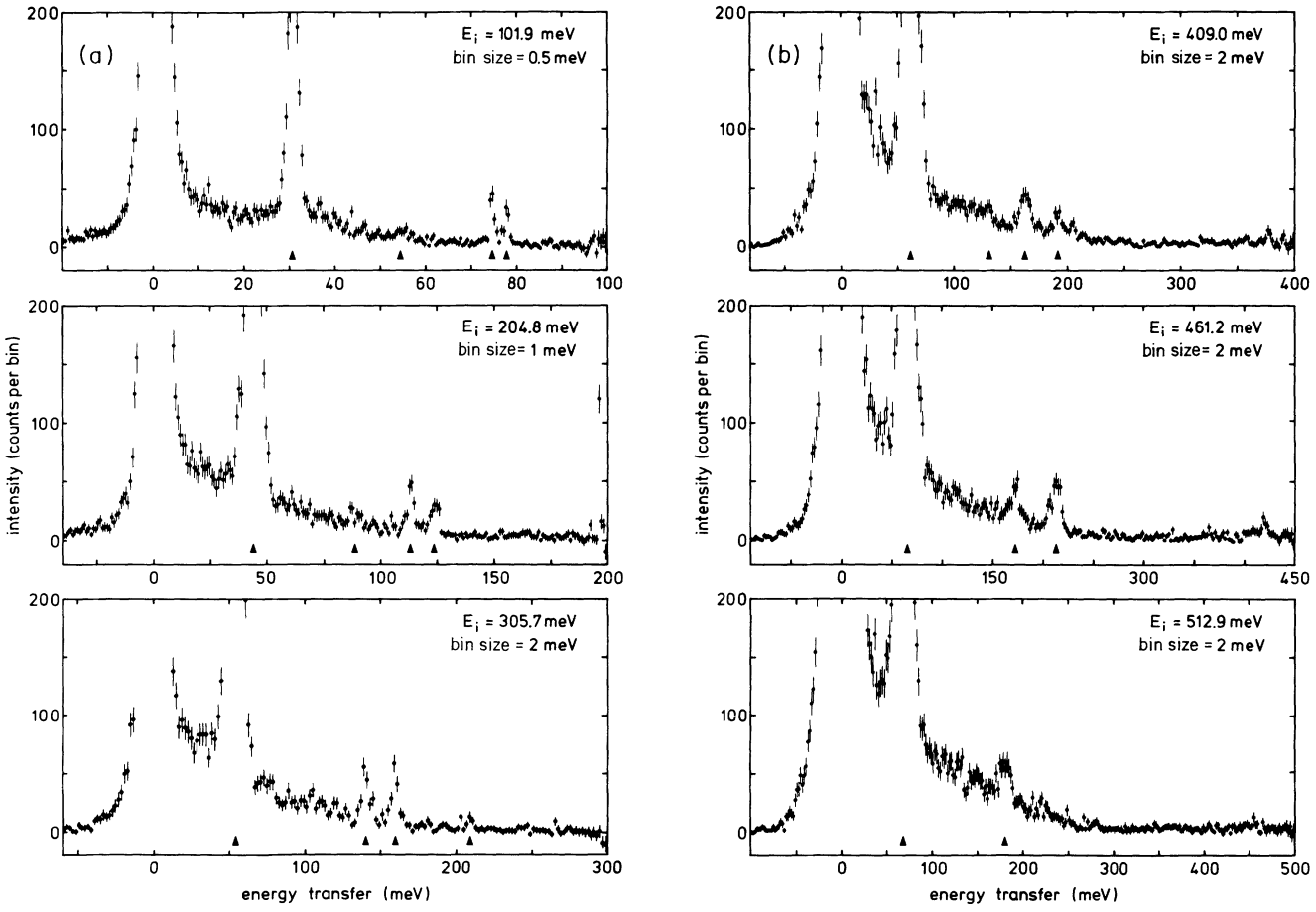

FIG. 2. Background-corrected TOF spectra taken on $KFeS_2$ at 10.7 K, accumulated over ≈ 1000 μA h proton charge ($E_i=513$ meV: ≈ 1500 μA h) and combining all available detectors with scattering angle 2θ below $\approx 10°$. Presumed spin-wave peaks that allowed fitting with an acceptable width are marked, the clipped ones are well described by simple Gaussians. Spikes at high energy transfer arise from time frame overlap.

TABLE II. Spin-wave energies representing peaks in the TOF spectra that allowed stable fits yielding an acceptable width, along with calculated longitudinal momentum transfers averaged over the detector area with proper weighting. The reduced values (1 r.l.u.$=2\pi/c$) are derived with the fitted periodicity parameter $C=c/2=2.686$ Å.

E_i (meV)	E (meV)	$\langle k \rangle$ (Å^{-1})	$\langle k \rangle_{red}$ (r.l.u.)	E (meV)	$\langle k \rangle$ (Å^{-1})	$\langle k \rangle_{red}$ (r.l.u.)
101.9	30.7	1.189	0.017	54.5	2.264	−0.064
	74.6	3.409	−0.086	77.8	3.626	0.100
204.8	43.7	1.183	0.011	88.6	2.503	0.140
	113.2	3.338	−0.146	123.5	3.722	0.182
305.7	54.0	1.196	0.023	139.9	3.260	−0.213
	159.3	3.798	0.247	209.3	5.371	−0.408
409.0	61.3	1.176	0.006	130.8	2.538	0.170
	162.3	3.210	−0.256	191.4	3.868	0.307
461.2	65.2	1.181	0.010	172.4	3.190	−0.272
	213.0	4.047	0.460			
512.9	68.4	1.177	0.006	180.4	3.146	−0.311

The detector banks of MARI involve ^{3}He-filled tubes arranged in linear arrays along circular arcs. If the position of any detector element is denoted by the distance x from the center of the tube concerned, which, in turn, is specified by the distance y along the arc from the forward position (Fig. 3), the scattering angle 2θ and azimuthal direction ϕ for this element are given by

$$\cos 2\theta = \frac{\cos(y/l)}{[1+(x/l)^2]^{1/2}}, \qquad \tan(\phi-\phi_0) = \frac{x/l}{\sin(y/l)}, \tag{2}$$

where $l=402$ cm is the distance sample detector, and ϕ_0 the azimuthal orientation of the detector bank. Knowing $2\theta(x,y)$, from (1) we may find the scattering-vector components $k_\parallel$ and $k_\perp$ and with these and the angle ϕ obtain the signal intensity $I(x,y)$ in dependence on spin orientation and magnetic form factor for each detector bank. Here, for $KFeS_2$, we have used the Hartree-Fock $3d$ form factor for spherical Fe^{3+} given in Ref. 18.

As a second deconvolution step, for each peak energy observed in the TOF scans, the corresponding longitudinal momentum transfer has been evaluated as an average

$$\langle k_\parallel \rangle = \frac{\int\int k_\parallel(x,y) I(x,y)\,dx\,dy}{\int\int I(x,y)\,dx\,dy} \tag{3}$$

over the active detector area, with the angle y/l ranging from 3.4° to 9.4°, and x from −15 to +15 cm, on each bank. The values obtained for the $KFeS_2$ spin-wave peaks are given in Table II and the E-k data points are graphically shown in Fig. 4. [A slightly increasing flight distance and decreasing visibility towards the ends of the tubes can be safely ignored in (3).]

For our measurements, the systematic corrections to $\langle k_\parallel \rangle$ arising in (3) from the variation of the signal intensity $I(x,y)$ over the detector area turn out to be below ≈ 0.01 Å^{-1}, which is the order of the statistical error in $k_\parallel$ introduced by uncertainties in the fitted peak energies, $\Delta k_\parallel = (dk_\parallel/dE)\Delta E$. Accordingly, the quality of definition and characteristic parameters of the spin-wave dispersion hardly change if $\langle k_\parallel \rangle$ is evaluated for $I(x,y)=1$. (Similarly, with no visible effect on the values in Table II, the magnetic moments in $KFeS_2$ can be taken

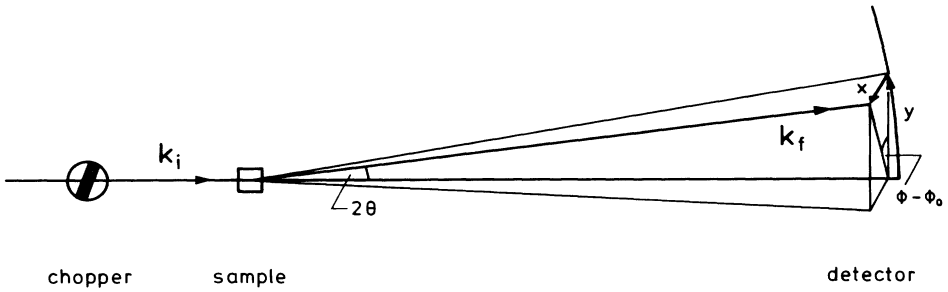

FIG. 3. Scattering geometry of a direct-geometry chopper spectrometer, defining the coordinates used for integrating over the detector banks of MARI. On each bank, a detector element is given by the distance x from the center of a ^{3}He tube, and the position y of the tube on a circular support.

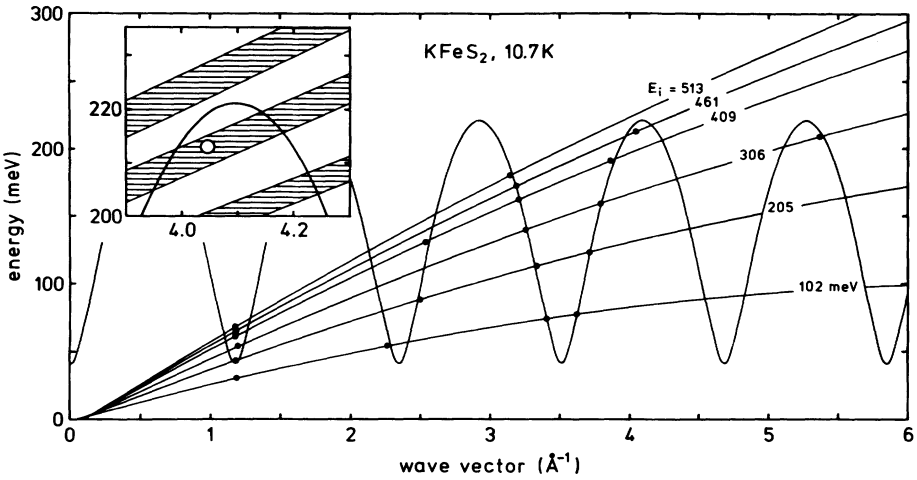

FIG. 4. $KFeS_2$ spin-wave dispersion fitted to the measured peak energies arranged along averaged TOF parabolas for the active detector area. The inset magnifies the region of the fourth maximum, where hatching denotes the E-k domains detected for the upper incident energies. A Néel-state magnon linewidth below ± 10 meV is implied by the absence of definite scattering for $E_i = 513$ meV.

parallel to the chain direction, which removes the dependence on the orientation ϕ_0 of the detector banks.) Thus, the use of a constant $I(x,y)$ in (3) should often be sufficient in practice; in this case, $\langle k_{\parallel} \rangle$ can simply be calculated from Eq. (1) with an effective scattering angle $2\theta_{\text{eff}}$ that is independent of k_i or k_f, $\cos(2\theta_{\text{eff}}) = \langle \cos 2\theta \rangle$. For our detection area, $2\theta_{\text{eff}}$ evaluates to 6.74°, while the actual effective angles for the $KFeS_2$ data points range from 6.35° to 6.71°.

IV. RESULTS

By means of a conventional least-squares adjustment, the data points of Table II were fitted with the dispersion relation appropriate for a 1D Heisenberg antiferromagnet,[14,15]

$$E(k) = \sqrt{A^2 + B^2 \sin^2(Ck)} \ , \tag{4}$$

where A provides for a finite energy gap and k stands for the longitudinal momentum transfer in units of Å^{-1}. In the fit, the obviously unresolved points from the first minimum ($k \approx 2\pi/c$) were excluded and the remaining 15 points given equal weights; the resulting parameter values are listed in Table III. The periodicity parameter C is in good agreement with the prediction from the x-ray lattice constant,[12,13] $C = c/2 = 2.695$ Å (a slight reduction is to be expected from lattice contraction at 10.7 K), and the fitted value has been used to map the data into the 1D antiferromagnetic Brillouin zone $-\pi/c < k < +\pi/c$ (Fig. 5). On the expanded scale of Fig. 5 it is evident that the model relation (4) provides a satisfactory description of the 1D spin-wave dispersion of $KFeS_2$, the statistical significance of the zone-center gap of $E(0) = A = 41(7)$ meV being apparent from the data themselves as well as from the parameter error.

In order to examine the influence of the less reliable peaks from the second and fifth dispersion valleys, the respective four data points were excluded in a repeated fit, which resulted in $A = 48(6)$ meV, $B = 215(4)$ meV, $C = 2.685(3)$ Å, $E(0)$ being slightly higher but the zone-boundary energy $E(\pi/c)$ almost unchanged. Similarly, without the top data point from the fourth period, in which two peaks are likely to coalesce, $E(\pi/c)$ increases

TABLE III. Spin-wave energy and periodicity parameters in the dispersion relation $E(k) = [A^2 + B^2 \sin^2(Ck)]^{1/2}$ fitted to data points obtained from the TOF spectra of $KFeS_2$ at 10.7 K. The energy gap $E(0) = A$ is attributed to the interchain dispersion averaged over the detector.

A (meV)	B (meV)	C (Å)
41(7)	217(4)	2.686(4)

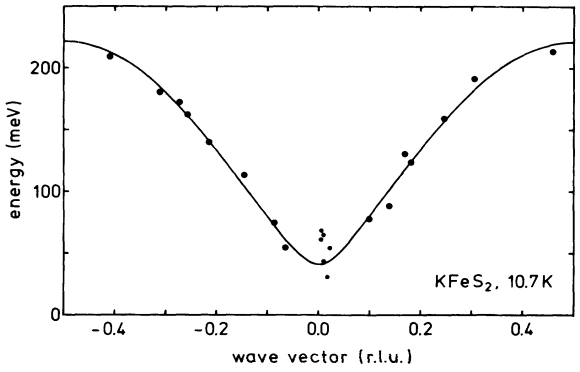

FIG. 5. Expanded view of the data mapped into the first 1D antiferromagnetic Brillouin zone (1 r.l.u. $= 2\pi/c$), with the fitted spin-wave dispersion. The cluster of points represented by smaller dots are from the unresolved first peaks in the TOF scans and were omitted in the fit. The gap $E(0) = 41(7)$ meV arising from the interchain dispersion is statistically significant.

only by about 2 meV. Substituting $k-k_0$ for k in relation (4) revealed no systematic shift of origin, $k_0=0.00(3)$ Å^{-1}, but gave a corresponding large error for C. Finally, if the detector integration (3) is performed with $I(x,y)=1$, a slightly smaller periodicity parameter $C=2.683(4)$ Å is obtained, the change being within the error margin. Clearly, the parameters in Table III may be considered representative of our data for $KFeS_2$.

The zone-boundary magnon energy in $KFeS_2$ obtained from the fit, $E(\pi/c)=(A^2+B^2)^{1/2}=221(4)$ meV (Table III), is about twice as large as expected from the earlier experiments with thermal neutrons[1] and close to the extrapolated result 204(11) meV for $TlFeS_2$;[2] we stress that, in the present work, the unusually high spin-wave energies in the Fe-S tetrahedral chains are established by a direct measurement. At the fourth dispersion period, the fitted zone-boundary energy is bracketed by the two uppermost TOF scans (Fig. 4, inset), which is directly confirmed by the sudden disappearance of the corresponding spin-wave signal for the highest incident energy (Fig. 2). From this, the magnon linewidth at the zone boundary is immediately seen to be less than about ± 10 meV in the Néel state. The observation of sharp spin-wave energies corroborates a local-moment behavior and a nonmetallic electronic state in the Fe-S chains of $KFeS_2$.

In the light of the thermal-neutron data,[1] the $KFeS_2$ zone-center gap of 41(7) meV can be attributed to the interchain dispersion which is integrated here over the detector area. Yet, because the gap is larger than anticipated from spin-wave energies found[1] not to reach above ≈ 19 meV along the b^* direction, much higher energies have to be suspected in the a^* direction. In fact, energies comparable to those measured[2] in $TlFeS_2$, of the order 40 meV, are also implied by the Oguchi relation[19] which relates the interchain dispersion to the Néel temperature [$T_N=196$ K for $TlFeS_2$ is somewhat lower[2]]. With $k_\perp$ [Eq. (1)] for $E_f\approx 100$ meV ranging from ≈ 0.4 to ≈ 1.1 Å^{-1}, the lateral integration typically covers more than one period of $a^*=0.964$ Å^{-1} or $b^*=0.558$ Å^{-1}, and even for our lowest $E_f\approx 25$ meV from the third longitudinal dispersion valley, a minimum as well as maximum along the a^* direction are probed by detectors.

The suspected origin of the gap is borne out by examining (Fig. 6) the integrated intensity of the first spin-wave peaks as a function of detector angle on the left-hand bank, which points roughly along the a^* axis. For the lower incident energies, the signal disappears where the interchain dispersion rises above the scan path, demonstrating that, around $h=0.5$, the dispersion reaches beyond 43.7 meV, but not much above 54.0 meV. Note that zero-angle scattering probes at $(-0.518,0,1)$ rather than the 3D antiferromagnetic Γ point (001), since the c^* direction in monoclinic $KFeS_2$ does not coincide with the chain axis. As a result of the neutron energy loss, the inelastic detector scans are slightly expanded with respect to the elastic reference signals also shown [the (110) reflection appears here because the detector tubes cover a broad strip in the a^*-b^* plane that makes an angle of about 20° with the a^* axis]. In accordance with Ref. 1, at

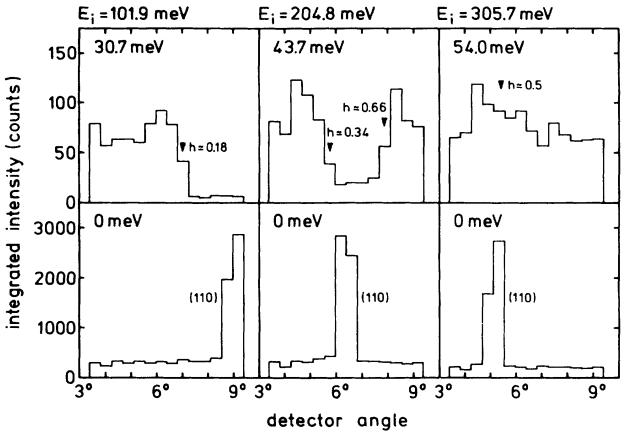

FIG. 6. Integrated intensity of the first spin-wave peaks and elastic peaks vs detector angle, along the left-hand bank pointing $\approx 20°$ off the a^* direction in the a^*-b^* plane, for the lower incident energies. Zero angle for the inelastic scans corresponds to $(-0.518,0,1)$. Where the interchain dispersion rises above the TOF path, the spin-wave signal disappears around $h=0.5$.

30.7 meV and above, the up and down detector banks show no comparable sharp features for the b^* direction, but up to 54.0 meV give reduced average intensities because of their width. The lateral energy modulation should contribute, along with the insufficient spectrometer resolution, to the fact that the longitudinal dispersion is completely unresolved in the first spin-wave peaks.

Relative to the low-temperature spectrum for $E_i\approx 300$ meV (Fig. 2), the corresponding room-temperature spectrum of $KFeS_2$ reveals no significant changes in the spin-wave or background signal, apart from the expected effects on signal intensity of the Bose factor, readily seen from energy-gain scattering around $E=-60$ meV, and of the random orientation of spins in the paramagnetic state above T_N. (As compared to spins aligned with the forward direction, a factor-of-$\frac{3}{2}$ decreased intensity is predicted in forward spin-wave scattering, but over the actual detector area the ratio reduces to 1.13 for the 54-meV peak, and here just balances the temperature effect.) In particular, the statistical quality of the present data does not permit any traces of a magnon continuum to be identified of the kind known from the $S=\frac{1}{2}$ paramagnetic Heisenberg chain.[20,21] Moreover, the peak shifts that would result from lattice expansion are too small to be confirmed reliably.

V. CONCLUSION

On the chopper spectrometer MARI, the antiferromagnetic spin-wave dispersion of $KFeS_2$ could easily be followed up to the zone boundary and a tight limit on the linewidth be obtained, in spite of the strong decrease in scattering cross section with increasing spin-wave energy. Clearly, it is crucial for the success of the experiment that, for a 1D system, an extended detection area can be utilized. One may suspect that these measurements would be less easy to perform with a triple-axis instrument fed by a conventional hot source in a high-flux reac-

tor than they are at ISIS.

A simple stepwise deconvolution scheme has been developed to derive the 1D dispersion curve from the data, and turns out to be adequate in view of the present instrument and experiment characteristics, with the resulting E-k data points being of remarkable precision. The scheme is easy to implement with moderate computing resources, its most noticeable shortcomings being an improper treatment of nonlinearities in the dispersion relation and difficulties with unseparated peaks (both of which occur near the zone boundary).

For our kind of experiment, an approximately fivefold gain in performance is to be anticipated if MARI is equipped with a full low-angle detector (factor ≈ 2.5) and a standard uranium target used (factor ≈ 2), which should, in principle, allow the present measurements to be performed in one day. Another substantial gain will result from the planned doubling of the ISIS mean proton current to 200 μA and raising the proton energy to the design value of 800 MeV. On the other hand, the usable intensity may be increased by relaxing the instrumental resolution, as, for instance, by widening the transmitted time window of the Fermi chopper.[22]

A complementary experiment for the related Tl compound,[10,2] which from $KFeS_2$ is distinguished by a bright silver-metallic appearance, would certainly be of interest.

ACKNOWLEDGMENTS

We wish to thank A. D. Taylor for making these measurements possible during the testing phase of MARI. The help of Z. A. Bowden and S. M. Bennington with the sample holder construction, goniometer and refrigerator installation, and spectrometer operation is gratefully acknowledged. We were much inspired by earlier measurements on $CsVCl_3$ performed on INC, National Laboratory for High-Energy Physics, Tsukuba, the results of which K. Kakurai made freely available to us. One of us (D.W.) received financial support from the Japan Society for the Promotion of Science (JSPS).

*Present address: Hahn-Meitner-Institut, Postfach 390128, D-1000 Berlin 39, Germany.

†Permanent address: National Laboratory for High Energy Physics, Tsukuba-shi, Ibaraki-ken 305, Japan.

[1]M. Nishi, Y. Ito, and S. Funahashi, J. Phys. Soc. Jpn. **52**, 2210 (1983).

[2]D. Welz and M. Nishi, Phys. Rev. B **45**, 9806 (1992).

[3]T. G. Perring, Ph.D. thesis, Cambridge University, 1991; T. G. Perring *et al.* (unpublished).

[4]D. Welz, M. Arai, M. Nishi, M. Kohgi, and Y. Endoh, in Proceedings of the International Conference on Neutron Scattering, Oxford, 1991 [Physica B (to be published)].

[5]A. D. Taylor *et al.*, in *Proceedings of the 11th Meeting of the International Collaboration on Advanced Neutron Sources, Tsukuba, 1990,* edited by M. Misawa *et al.* (National Laboratory for High-Energy Physics, Tsukuba, 1991), p. 705; M. Arai *et al.*, *ibid.*, p. 644.

[6]L. J. de Jongh and A. R. Miedema, Adv. Phys. **23**, 1 (1974).

[7]M. Steiner, J. Villain, and C. G. Windsor, Adv. Phys. **25**, 87 (1976).

[8]M. Nishi and Y. Ito, Solid State Commun. **30**, 571 (1979).

[9]Z. Tomkowicz, A. Szytula, and H. Bak-Ptasiewicz, Phys. Status Solidi A **57**, K25 (1980).

[10]D. Welz, P. Deppe, W. Schäfer, H. Sabrowsky, and M. Rosenberg, J. Phys. Chem. Solids **50**, 297 (1989).

[11]D. O. Cowan, G. Pasternak, and F. Kaufman, Proc. Nat. Acad. Sci. (U.S.A.) **66**, 837 (1970).

[12]J. W. Boon and C. H. MacGillavry, Rec. Trav. Chim. Pays-Bas **61**, 910 (1942).

[13]W. Bronger, Z. Anorg. Allg. Chem. **359**, 225 (1968).

[14]R. Kubo, Phys. Rev. **87**, 568 (1952).

[15]F. Keffer, in *Handbuch der Physik,* edited by S. Flügge (Springer-Verlag, Berlin, 1966), Vol. XVIII/2, pp. 1–273.

[16]See, for example, S. W. Lovesey, *Theory of Neutron Scattering from Condensed Matter* (Clarendon, Oxford, 1984), Vol. 2.

[17]R. Osborn (unpublished).

[18]R. E. Watson and A. J. Freeman, Acta Crystallogr. **14**, 27 (1961).

[19]T. Oguchi, Phys. Rev. **133**, A1098 (1964).

[20]I. U. Heilmann, G. Shirane, Y. Endoh, R. J. Birgeneau, and S. L. Holt, Phys. Rev. B **18**, 3530 (1978).

[21]J. C. Bonner, in *Magnetostructural Correlations in Exchange Coupled Systems,* edited by R. D. Willett *et al.* (Reidel, Dordrecht, 1985), pp. 157–205.

[22]A. D. Taylor (private communication).